

## MIT Open Access Articles

*Control of zinc oxide nanowire array properties with electron beam lithography templating for PV applications*

The MIT Faculty has made this article openly available. **Please share** how this access benefits you. Your story matters.

**Citation:** Nicaise, Samuel M, Jayce J Cheng, Amirreza Kiani, Silvija Gradecak, and Karl K Berggren. "Control of Zinc Oxide Nanowire Array Properties with Electron-Beam Lithography Templating for Photovoltaic Applications." *Nanotechnology* 26, no. 7 (February 2, 2015): 075303.

**As Published:** <http://dx.doi.org/10.1088/0957-4484/26/7/075303>

**Publisher:** IOP Publishing

**Persistent URL:** <http://hdl.handle.net/1721.1/99748>

**Version:** Author's final manuscript: final author's manuscript post peer review, without publisher's formatting or copy editing

**Terms of use:** Creative Commons Attribution-Noncommercial-Share Alike



# Control of zinc oxide nanowire array properties with electron beam lithography templating for PV applications

Samuel M. Nicaise<sup>1\*</sup>, Jayce J. Cheng<sup>2\*</sup>, Amirreza Kiani<sup>2,3</sup>, Silvija Gradečak<sup>2</sup>, Karl Berggren<sup>1</sup>

<sup>1</sup>Department of Electrical Engineering and Computer Science, <sup>2</sup>Department of Materials Science and Engineering, Massachusetts Institute of Technology, Cambridge, MA 02139, USA, <sup>3</sup>Department of Electrical Engineering, University of Toronto, Toronto, ON, M5S3G4, Canada

\*These authors contributed equally to this work

E-mail: berggren@mit.edu

## Abstract

Hydrothermally synthesized zinc oxide nanowire arrays have been used as nanostructured acceptors in emerging photovoltaic (PV) devices. The nanoscale dimensions of such arrays allow for enhanced charge extraction from PV active layers, but the device performance critically depends on the nanowire array pitch and alignment. In this study, we templated hydrothermally-grown ZnO nanowire arrays via high-resolution electron-beam-lithography defined masks, achieving the dual requirements of high-resolution patterning at a pitch of several hundred nanometers, while maintaining hole sizes small enough to control nanowire array morphology. We investigated several process conditions, including the effect of annealing sputtered and spincoated ZnO seed layers on nanowire growth, to optimize array property metrics – branching from individual template holes and off-normal alignment. We found that decreasing template hole size decreased branching prevalence but also reduced alignment. Annealing seed layers typically improved alignment, and sputtered seed layers yielded nanowire arrays superior to spincoated seed layers. We show that these effects arose from variation in the size of the template holes relative to the ZnO grain size in the seed layer. The quantitative control of branching and alignment of the nanowire array that is achieved in this study will open new paths toward engineering more efficient electrodes to increase photocurrent in nanostructured PVs. This control is also applicable to inorganic nanowire growth in general, nanomechanical generators, nanowire transistors, and surface-energy engineering.

**Keywords:** ZnO nanowires, hydrothermal growth, electron-beam lithography, nanowire alignment, nanostructured photovoltaics

## 1. Introduction

The use of inorganic nanostructure arrays in emerging photovoltaic (PV) devices has recently garnered much interest because the nanostructures present opportunities to mediate charge transport at the nanoscale [1,2]. Bulk heterojunction PV devices utilizing zinc oxide nanowire arrays have shown high performance when prepared in conjunction with a variety of active materials including P3HT [3,4], PCBM:P3HT [5,6], CdS [7,8], dye-sensitizers [9,10] and colloidal quantum dot (QD) thin films [1]. The minority carrier diffusion length in the active material of these devices lies in the nano- to micrometer length scale. As such, provision of a nanostructured scaffold, e.g. ZnO nanowire array, can greatly aid charge extraction [1]. Unlike other nanowire scaffold materials like TiO<sub>2</sub> [11,12], hydrothermally synthesized ZnO nanowire arrays are favorable because they can be grown at low temperature and moderate pH [13] on a variety of substrates [4,14], with substantial control over morphology [15].

ZnO nanowire arrays, as shown in Figure 1a, have been successfully used to enhance QD-based PV device performance [16–18]. However, a compromise exists between charge generation (high QD fill factor) and charge extraction (high scaffold density) when designing the geometry of the nanostructured scaffold acceptor because of effects on current density and consequently device power conversion efficiency. Maximizing the QD fill factor increases the current density because absorption of incident light occurs primarily in the QD film. Larger nanowire pitches allow for a higher QD fill factor and decrease void formation in the QD layer, thus increasing light absorption. However, if the nanowire pitch is too large, the disparity between collection length (several hundred nm) and absorption length (~1 μm) results in regions of poor charge collection, or ‘dead zones’ [19]. Orthogonalizing control of the collection and generation length scales thus allows more carriers to be collected compared to the equivalent thin-film device; recent simulations of nanopillar QD PV devices performed by Kramer *et al.* suggest that current density would be maximized at a nanowire array pitch of 276 nm [20] for MPA-treated PbS QDs. The ability to control nanowire pitch between 200 – 300 nm would thus be useful for increasing QD PV power conversion efficiency.

Considering the aforementioned compromise, we present in Figure 1a drawing of the ideal nanowire array as part of a QD PV device and an experimental example of a ZnO nanowire array in which the pitch is precisely controlled. While previous reports of templated ZnO nanowire arrays have controlled array pitch [21–25], these reports did not simultaneously achieve (1) small template-hole diameter for single-nanowire growth and (2) high-resolution pitch-control for optimized charge collection. These characteristics are required to grow single nanowires at precise positions for maximum charge collection. Furthermore the profound effect of the ZnO seed layer on nanowire morphology makes it a key processing parameter, and yet quantitative studies are lacking. In general, previous reports have observed high quality ZnO nanowire array growth on sputtered seed layers [26–28] but array quality is inconsistent for nanowires grown on spincoated seed layers [29,30]. Nanowire array engineering for PV device, piezoelectric [31] and field-emitter [32] applications will require quantitative study of the effect of processing conditions on array properties, specifically on branching (multiple nanowires growing from a single template hole) and on nanowire alignment.

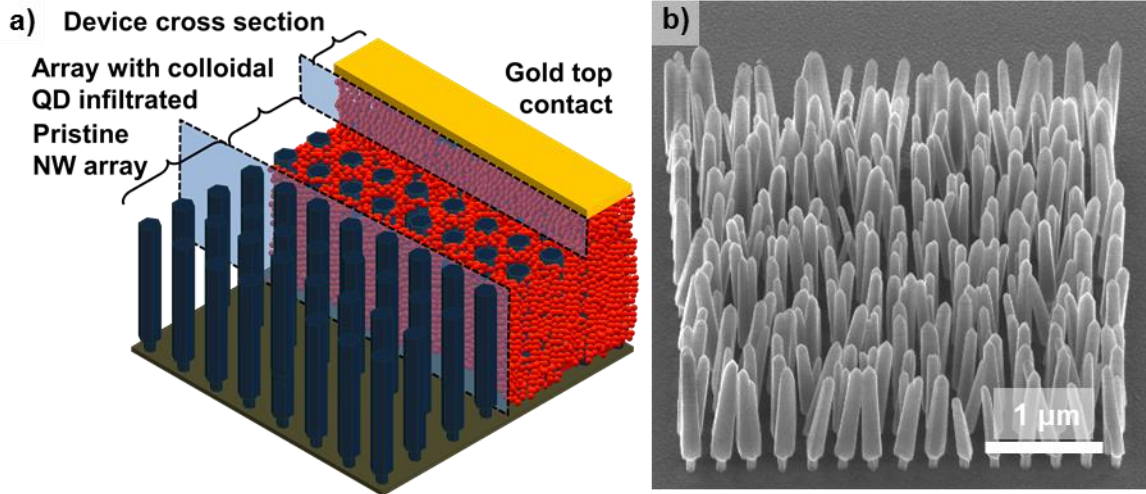


**Figure 1: ZnO nanowire arrays for QD-based PV devices.** (a) Schematic of an ideal templated nanowire array for bulk heterojunction QD-based PV device. For demonstrative purposes, the array is void of QDs in the front of the array, infiltrated with colloidal QDs (red) in the middle of the array, and has the full QD PV device cross section with gold top contact (yellow) at back. QDs are not to scale. (b) Scanning-helium-ion micrograph (45° tilt) of a templated ZnO nanowire array without infiltrated QDs.

Here, we focus on controlling the branching and alignment of ZnO nanowire arrays fabricated by electron-beam lithography (EBL) and hydrothermal synthesis at the length scales that are relevant for

nanowire-based QD PV devices. We specifically focus on the following process parameters: substrate, seed layer deposition and annealing, and template hole size. Templated nanowire arrays were grown on silicon, indium tin oxide-coated glass (ITO/glass) and poly(ethylene naphthalate) (PEN) substrates. ZnO seed layers, deposited by sol-gel spincoating or sputter deposition, and either thermally annealed or used as-deposited, were templated at a near-ideal pitch of 276 nm via an EBL-fabricated growth mask. The degree of branching and alignment were used as figures of merit to determine the quality of the fabrication process. We found that annealing of the seed layer improves nanowire array alignment for the spincoated seed layer deposition process. Arrays grown on sputtered seed layers show superior alignment compared to those grown on spincoated seed layers, while both show similar degrees of branching. The choice of substrate used in this work contributes minimally to nanowire array quality. Consequently, the process outlined here may be applicable to a wide range of substrate materials, thus supporting scalability of the process. Control via template hole diameter is particularly dependent on the method for seed layer deposition – while a decrease in hole diameter decreases branching, smaller holes result in poorer alignment for spincoated seed layers but have no effect on sputtered seed layers. We suggest that array control can be achieved with engineered template hole size relative to seed layer grain size, and explain our results based on this hypothesis.

## **2. Experimental details**

The EBL-templated hydrothermal growth process used in this work is shown in Figure 2. ZnO nanowire arrays were grown hydrothermally after using EBL to define templates on both sputtered and spincoated seed layers. The nanowire arrays were then inspected with either scanning electron microscopy (SEM) or helium ion beam microscopy (HIM), and images were analyzed to extract branching and alignment metrics.

### *2.1 Templated growth*

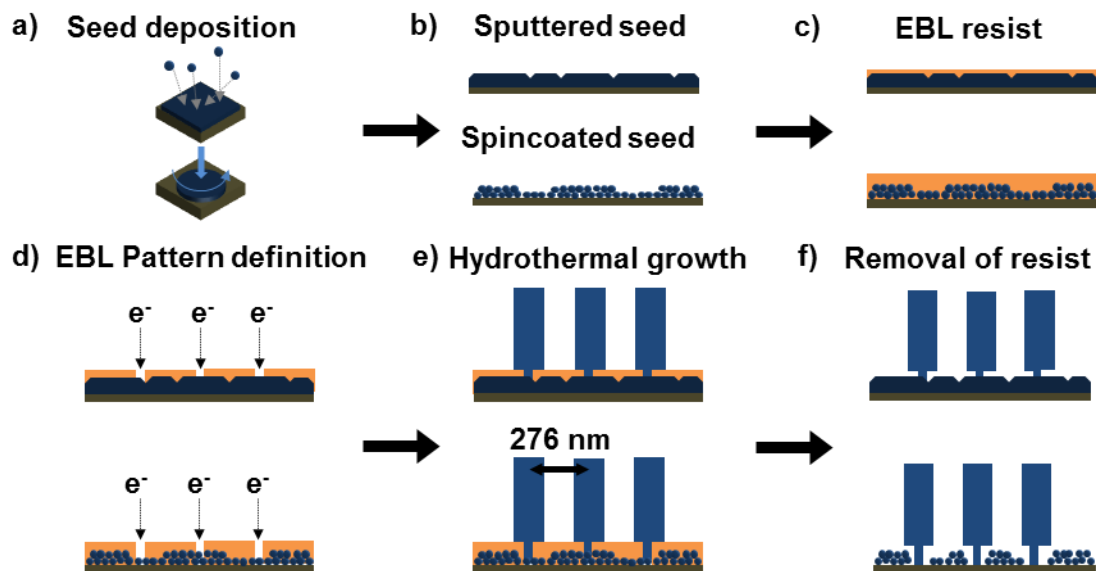


**Figure 2: EBL fabrication process for templated hydrothermal ZnO growth.** (a) ZnO seed layer deposition either by sputtering (top) or spincoating from solution (bottom), (b) some of the samples were annealed at 400°C for 2 h while others were not annealed, (c) PMMA resist was spincoated and then (d) templating holes were defined by EBL, (e) nanowires grew through the template holes in the hydrothermal growth solution, and (f) oxygen plasma etching removed the remaining PMMA and exposed the bases of the nanowires. Colors: gray is the substrate, blue is ZnO, and orange is the PMMA resist.

As shown in Figure 2a, ZnO seed layers were first deposited on Si (111), ITO/glass, and PEN substrates by spincoating or sputtering. Si substrates have low surface roughness and were used as a baseline for high quality nanowire growth. ITO/glass is a common conducting substrate used for PV device electrodes, and PEN was chosen for its thermal properties to represent a possible flexible PV substrate. Spincoated layers were deposited from a solution of 0.3 M zinc acetate/monoethanolamine (1:1) in 2-methoxyethanol at 4000 rpm, for 60 sec and annealed at 175°C for 10 min; this process was repeated to produce a ZnO thickness of ~30 nm. RF-sputtered ZnO films were deposited by using an AJA Orion 5 at 100 W, 3 mT Ar for 24 min for a thickness of ~180 nm. Seed layers were then annealed on a hotplate at 400°C in ambient atmosphere for 2 h (Figure 2b).

Poly(methyl methacrylate) electron-beam resist (4% dilution, 950PMMA A MicroChem) was spincoated (shown in Figure 2c) at 4000 rpm for 60 sec, followed by a post-bake at 85°C for 2 min (below the PMMA glass transition temperature, for solvent evaporation), and measured to be ~100 nm thick via ellipsometry. As shown in Figure 2d, a Raith 150 electron-beam lithography tool was used to write a 15 × 15 square array of circles at a pitch of 276 nm (~300 pA, 30 keV, 6-mm working distance).

The electron-beam dose for each exposure varied from 100 to 40,000  $\mu\text{C cm}^{-2}$ . After the lithography step, samples were developed at 24°C in a solution of 3:1 isopropanol (IPA):methyl isobutylketone (MIBK) for 1 min, rinsed with IPA for 1 min, and blown dry under nitrogen flow. As PMMA is a positive tone resist at the delivered dose, the development solution dissolved the areas exposed by the electron beam to leave behind holes in the PMMA film, exposing the underlying ZnO seed layer.

Pictured in Figure 2e, hydrothermal growth of ZnO nanowires was performed by suspending patterned substrates face down in an aqueous growth solution (MilliQ 18 M $\Omega$ ) consisting of 25 mM zinc nitrate, 25 mM hexamethylene tetramine and 5 mM polyethyleneimine (Sigma-Aldrich) at 90°C for 100 min. Oxygen plasma etching was then used to remove the PMMA mask, leaving lithographically-defined nanowire arrays (Figure 2f).

A Zeiss Orion HIM operating at 35 kV and a working distance of 10 mm was used to image the resulting nanowire arrays (both top down and at 45° tilt) and pre-growth PMMA template hole arrays and seed layers. A Veeco Nanoscope IV atomic force microscope (AFM) was used for imaging of the ZnO seed layers in tapping mode with a standard Si tip.

## 2.2 Image analysis

Three morphological parameters were measured from micrographs in order to characterize the effects of process variables. First, prior to nanowire growth, we measured the diameter of templating holes, as the controlled experimental variable. The measurement was performed using a Matlab procedure (detailed in SI) from top-down micrographs of the resulting template hole arrays. For a given template array, the lithographic dose delivered to each hole location was designed to be the same. Hole diameters were averaged over each individual array to obtain the template hole diameter metric as the controlled variable.

Second, the degree of branching was determined by counting the number of branched nanowires from top-down micrographs. Figure 3a depicts branching, where an individual templating hole results in one or multiple emerging nanowires. In this report, we use the term “nonbranched” to describe a template hole that results in a single nanowire. Conversely, we use the term “branched” to describe a template hole that



results in two or more nanowires. For each array of nanowires, the prevalence of nonbranching was calculated as the number of nonbranched divided by the sum of branched and nonbranched holes. Holes without nanowires were excluded and this issue is discussed as nanowire array yield (see SI).

Lastly, we measured the alignment of the nanowires and calculated the order parameter as a quantitative metric. The Herman's order parameter  $S = \frac{3}{2} \langle \cos^2 \varphi \rangle - \frac{1}{2}$ , where  $\varphi$  is the deviation angle between the nanowire and the substrate normal, is a widely used measure of the preferential alignment [4,33,34]. As shown in Figure 3b,  $\varphi$  was measured from SEM micrographs of nanowire arrays taken at 45° tilt (see SI for a detailed description of measurement method and discussion of geometric transformation). For each array,  $S$  was calculated by averaging values for all nanowires in the array and it ranges between values of 1 for alignment normal to the substrate and -0.5 for alignment parallel with the substrate surface.

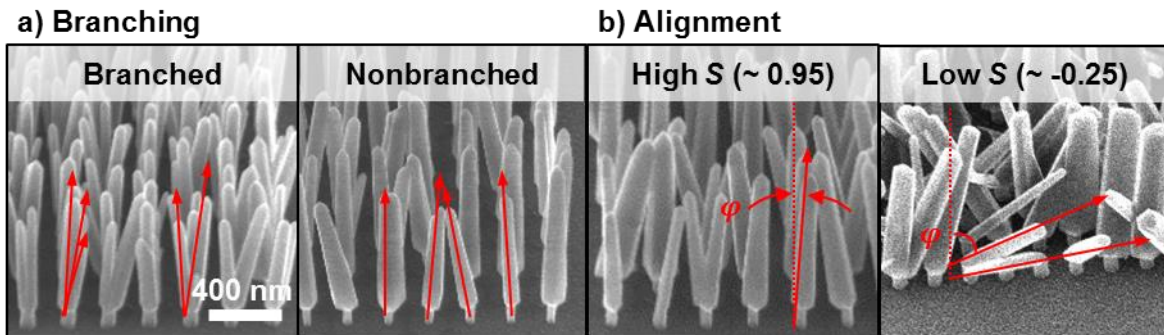


**Figure 3: Analysis of micrographs for nanowire branching and alignment.** (a) Micrographs of nanowires which exemplify branched (left) and nonbranched (right) arrays. (b) Micrographs of nanowires which exemplify high (left) and low (right) order parameter ( $S$ ). All micrographs are at the same scale.

### 3. Results and discussion

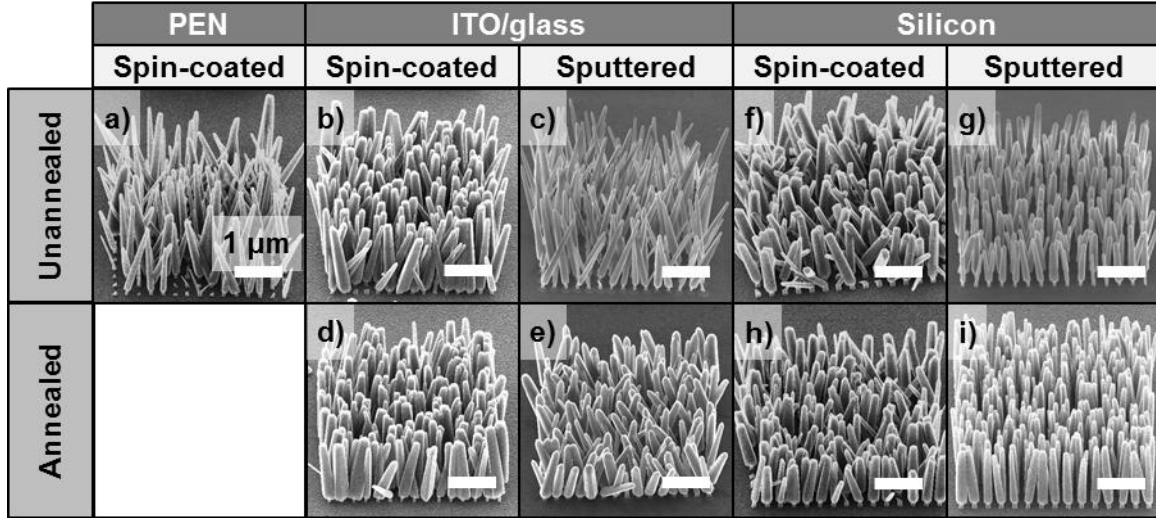


**Figure 4: Helium ion micrographs of 276-nm pitch templated nanowire arrays obtained at 45° tilt.** All micrographs were chosen as the most aligned and least branched example from each experimental process combination of substrate, seed layer deposition, and annealing. Note that template hole diameters are not identical for each image. Nanowire growth from an annealed seed layer on PEN was not tested. All scale bars are identical.

We demonstrate the growth of templated unbranched ZnO nanowire arrays with good alignment for all substrates, annealing conditions, coating processes, and a range of template hole diameters. Figure 4b – i show examples of nanowire arrays grown on Si and ITO/glass. Nanowire diameter is constricted at the base due to PMMA template confinement; unconstrained lateral growth takes place when the nanowire emerges above the template causing larger diameters (details in SI). Qualitatively, rigid substrates (Si and ITO/glass) result in less branched, more aligned nanowire arrays than flexible PEN substrates. The nanowires grown on Si and ITO/glass are comparable to recent high-resolution templating of hydrothermally-grown ZnO nanowires on Si, GaAs, GaN, and sapphire [22,23,35–37]. Photoluminescence performed on nanowire arrays displayed low defect intensity peaks (see SI), confirming good ZnO crystal quality. Nanowire alignment is marginally more orthogonal on Si as compared to ITO/glass substrates. Figure 4a shows that high resolution templated growth on flexible PEN substrates can be achieved, despite the non-conductive nature (and therefore difficult EBL) of PEN. Nevertheless, the reliability of the fabrication process for PEN substrates is lower than that for Si and ITO/glass. We attribute lower reliability to thermal degradation of the substrate, mechanical bending of

the substrate from thin film stress, difficulty in carrying out EBL on a non-conducting surface, and possibly, reduced adhesion energy between the ZnO nanowires and the substrate.

### *3.1 Effect of varying template hole size on branching*

Branching is theoretically detrimental to PV charge collection because multiple nanowires emerging from a single template hole negate the precise placement of individual nanowires, as engineered in the template. Additionally, branched and misaligned wire growth can reduce the QD volume in the film and generate voids in the film due to poor QD infiltration. Therefore, understanding and controlling nanowire branching and alignment is critical for future development of nanowire-based QD PV devices.

Figure 5a and b display plots of the frequency of non-branching nanowires versus the measured template hole size. We varied the template hole diameter between 50 and 100 nm, a length scale challenging for many lithography techniques. For clarity, spincoated (Figure 5a and c) and sputtered (Figure 5b and d) seed layers are separated, and templating hole diameters are binned in 10-nm intervals. In general, the frequency of branching can be controlled over the whole range of 0 – 100% and we accept >90% non-branched as an optimized array. Branching trends are similar for both sputtered and spincoated seed layers. A range of template hole sizes results in arrays that have low enough branching to be acceptable for device fabrication, but we always observe a decrease in branching as hole size decreases. Arrays on spincoated and sputtered seed layers behave differently when annealed – branching increases after annealing for spincoated seed layers (Figure 5a), whereas the opposite is true for sputtered seed layers (Figure 5b). We attribute this effect to mutual impingement and template confinement, which will be elaborated on subsequently.

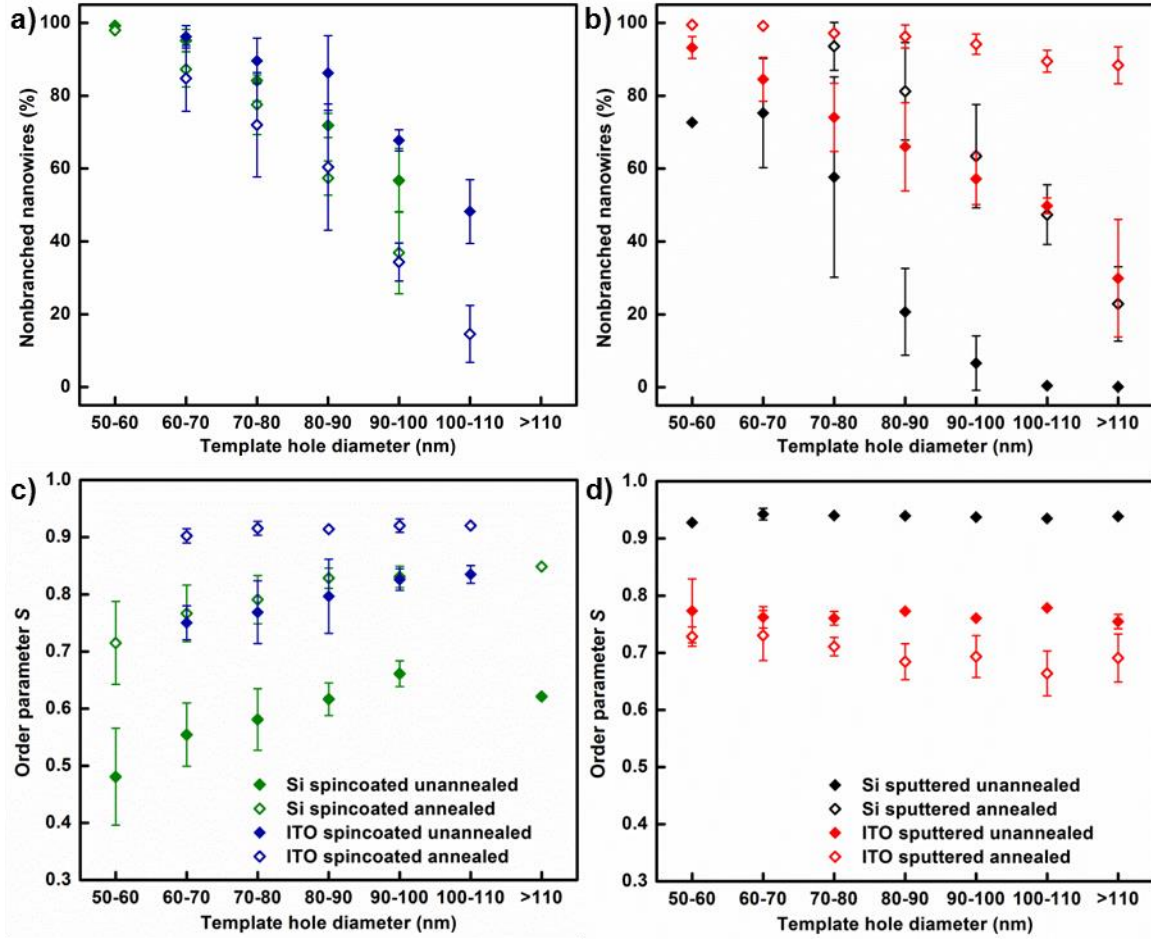


**Figure 5: Percentage of non-branched nanowires and alignment vs. template hole diameter.** (a) and (b) Percentage of non-branched nanowires as a function of template hole diameter. Percentage data points are plotted for each templating hole array of each respective measured templating hole diameter falling in the specific bin. (c) and (d) Plots of the order parameter  $S$  as a function of template hole diameter. Each data point is the average  $S$  for all of the templating arrays with measured hole diameter falling in the specific bin. Error bars are one standard deviation and omitted where smaller than symbol size.

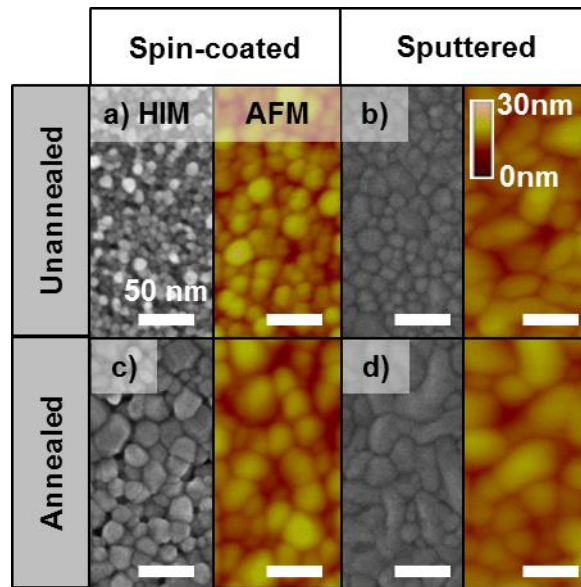
### 3.2 Effect of varying template hole size on alignment

Figure 5c and d display plots of order parameter,  $S$ , versus the measured template hole size. We observed two different trends depending on the nature of the seed layer: for spincoated seed layers (Figure 5c) the order parameter ranges from 0.5 to 0.9, whereas for sputtered seed layers (Figure 5d) the variation is much smaller, ranging from 0.65 to 0.98. For spincoated samples, nanowire alignment improves with increasing hole diameter, whereas there is little variation in alignment with changing hole diameter for sputtered samples.

### 3.3 Effect of annealing and template hole size on morphology

In addition to the strong effect that the size of the template hole has on array characteristics, annealing generally results in better nanowire alignment, although annealing increases branching in spincoated seed layers. Figure 5c shows that annealing spincoated seed layers results in more aligned nanowires. Figure 5d shows that annealing the sputtered seed layer on ITO/glass substrates only slightly affects alignment, which can be attributed to the already excellent alignment of the unannealed sputtered seed layer [26].

The results show that template hole size and annealing have a strong impact on branching and alignment. Branching has been shown to be affected by growth temperature [22] and concentration [38], seed alignment [23], seed density [27], seed nucleation and growth [39], and template hole size [40]. We suggest that the size of ZnO grains in the seed layer is the underlying factor that leads to the observed influence of template hole size and annealing on nanowire growth. As the template holes are expected to be larger than the ZnO grains in the seed layer, the number of exposed ZnO grains, and therefore the prevalence of branching, is a function of the respective sizes of the template hole and exposed ZnO grains. A precise measurement of ZnO grain sizes in the seed layer is thus necessary.



**Figure 6: HIM and AFM micrographs of ZnO seed layers on Si before hydrothermal growth.** Grayscale and colored images are HIM and AFM micrographs, respectively. Thermal annealing (bottom row), as opposed to no annealing (top row), increases the grain diameter. The diameters were measured from HIMs as (mean  $\pm$  standard

deviation) (a)  $7.5 \pm 2.0$ , (b)  $39.6 \pm 23.3$ , (c)  $21.7 \pm 8.9$ , and (d)  $51.2 \pm 16.1$  nm. All scale bars and vertical AFM scales are identical.

Figure 6 shows that seed layer grain size increases after annealing for both sputter-coating (from  $39.6 \pm 23.3$  to  $51.2 \pm 16.1$  nm) and spincoating ( $7.5 \pm 2.0$  to  $21.7 \pm 8.9$  nm). Template hole diameters typically range from 40 – 120 nm, which is larger than the grain diameters and thus multiple grains are exposed to the hydrothermal growth solution. Therefore, nanowire branching is reduced as the template hole diameter decreases because fewer ZnO grains are exposed to the growth solution. Annealing reduces overall branching for sputtered seed layers by increasing the ZnO grain size, though this does not apply to spincoated seed layers because the ZnO grains are much smaller than in sputtered seed layers. To explain increased branching for spincoated seed layers after annealing, we discuss the twofold effect of annealing in increasing grain size and enhancing seed layer alignment below.

Isolating the factors that explain the observed trends in alignment is more difficult because alignment is affected not only by the number of exposed grains, but also by seed layer texturing. In seeded growth, nanowires grow directly from the c-planes of individual ZnO grains in the seed layer, and therefore the texture of grains in the seed layer significantly alters the final nanowire alignment. ZnO films used as seed layers are typically annealed to improve their c-plane texturing with respect to the substrate [14,41], which is in agreement with our results where annealing generally improves nanowire alignment.

Furthermore, the prevalence of branching also changes nanowire density, which can affect alignment. Misaligned nanowires tend to impinge mutually and/or grow into the PMMA template sidewalls, preventing further growth and leaving only nanowires growing normal to the substrate [30]. In this report, alignment is a function of template hole diameter in samples with substantial nanowire branching and poor seed layer texturing, such as in spincoated seed layers (Figure 5c). As annealing improves grain alignment in highly misoriented spincoated seed layers, fewer nanowires impinge into PMMA sidewalls, causing branching to increase as more nanowires are able to grow vertically. This relationship suggests that the dependence of the order parameter on template hole diameter and branching are actually mutually

related, especially for spincoated seed layers where the grain sizes, whether annealed or unannealed, are much smaller than the template hole diameters (see SI for further discussion). On the other hand, the effect of nanowire density on order parameter is less pronounced in sputtered samples where seed layer texturing has already been enhanced (Figure 5d) and we therefore suggest nanowire density is too low for mutual impingement to have an effect. Finally, annealing also has the added effect of increasing the grain size and decreasing the nanowire density, which is in turn detrimental to nanowire alignment [15]; this could explain the marginally poorer alignment in annealed sputtered seed layers on ITO compared to unannealed seed layers (Figure 5d).

#### **4. Conclusion**

In conclusion, we show that lithographic masks can be used for high-resolution templated hydrothermal growth of ZnO nanowires and that the tested process parameters (substrate type, seed layer deposition, annealing, and template hole size) can control branching and nanowire alignment. We found that a well aligned ZnO nanowire array suitable for use in PV devices could be templated on an ITO/glass substrate on an annealed spincoated seed layer. This is the first example of EBL-templating of ZnO nanowires at high-resolution pitches suited to QD-based PV devices. Future research can pair larger ZnO seed layer grains with transparent or flexible substrates and take advantage of parallel lithographic approaches such as nano-imprint lithography [42], self-assembled microspheres [43] or low-cost optical interference lithography [44]. Beyond ZnO nanowire QD PVs, this work is widely applicable in other fields, such as nanomechanical energy generators, surface-energy engineering, nanowire transistors, and templated growth of other inorganic nanowires [45–48].

#### **5. Acknowledgements**

This work was supported by a Massachusetts Institute of Technology Energy Initiative Grant and the National Science Foundation Scalable Nanomanufacturing 12-544. S.M.N. was supported by a National Science Foundation Graduate Research Fellowship. J.J.C. acknowledges financial support from the

Agency for Science, Technology and Research, Singapore. Authors would like to thank Mark K. Mondol and James Daley of the MIT NanoStructures Laboratory for technical assistance. Authors would like to thank Drs. Richard Hobbs and Sehoon Chang for useful discussions and input.



## References

- [1] Jean J, Chang S, Brown P R, Cheng J J and Rekemeyer P H 2013 ZnO Nanowire Arrays for Enhanced Photocurrent in PbS Quantum Dot Solar Cells *Adv. Mater.* **25** 2790–6
- [2] Lan X, Bai J, Masala S, Thon S M, Ren Y, Kramer I J, Hoogland S, Simchi A, Koleilat G I, Paz-Soldan D, Ning Z, Labelle A J, Kim J Y, Jabbour G and Sargent E H 2013 Self-assembled, nanowire network electrodes for depleted bulk heterojunction solar cells. *Adv. Mater.* **25** 1769–73
- [3] Olson D C, Lee Y-J, White M S, Kopidakis N, Shaheen S E, Ginley D S, Voigt J a. and Hsu J W P 2008 Effect of ZnO Processing on the Photovoltage of ZnO/Poly(3-hexylthiophene) Solar Cells *J. Phys. Chem. C* **112** 9544–7
- [4] Park H, Chang S, Jean J, Cheng J J, Araujo P T, Wang M, Bawendi M G, Dresselhaus M S, Bulović V, Kong J and Gradečak S 2013 Graphene cathode-based ZnO nanowire hybrid solar cells. *Nano Lett.* **13** 233–9
- [5] Takanezawa K, Tajima K and Hashimoto K 2008 Efficiency enhancement of polymer photovoltaic devices hybridized with ZnO nanorod arrays by the introduction of a vanadium oxide buffer layer *Appl. Phys. Lett.* **93** 063308
- [6] Takanezawa K, Hirota K, Wei Q-S, Tajima K and Hashimoto K 2007 Efficient Charge Collection with ZnO Nanorod Array in Hybrid Photovoltaic Devices *J. Phys. Chem. C* **111** 7218–23
- [7] Wang L, Zhao D, Su Z, Li B, Zhang Z and Shen D 2011 Enhanced Efficiency of Polymer / ZnO Nanorods Hybrid Solar Cell Sensitized by CdS Quantum Dots *J. Electrochem. Soc.* **158** H804–H807
- [8] Feng Z, Zhang Q, Lin L, Guo H, Zhou J and Lin Z 2010 <0001>-Preferential Growth of CdSe Nanowires on Conducting Glass: Template-Free Electrodeposition and Application in Photovoltaics *Chem. Mater.* **22** 2705–10
- [9] Quintana M, Edvinsson T, Hagfeldt A and Boschloo G 2007 Comparison of Dye-Sensitized ZnO and TiO<sub>2</sub> Solar Cells : Studies of Charge Transport and Carrier Lifetime *J. Phys. Chem. C* **111** 1035–41
- [10] Saito M and Fujihara S 2008 Large photocurrent generation in dye-sensitized ZnO solar cells *Energy Environ. Sci.* **1** 280
- [11] Xu C and Gao D 2012 Two-Stage Hydrothermal Growth of Long ZnO Nanowires for Efficient TiO<sub>2</sub> Nanotube-Based Dye-Sensitized Solar Cells *J. Phys. Chem. C* **116** 7236–41
- [12] Quintana M and Edvinsson T 2007 Comparison of dye-sensitized ZnO and TiO<sub>2</sub> solar cells: studies of charge transport and carrier lifetime *J. Physical Chem. C* **111** 1035–41
- [13] Vayssieres L 2003 Growth of Arrayed Nanorods and Nanowires of ZnO from Aqueous Solutions *Adv. Mater.* **15** 464–6

- [14] Greene L E, Law M, Tan D H, Montano M, Goldberger J, Somorjai G and Yang P 2005 General route to vertical ZnO nanowire arrays using textured ZnO seeds *Nano Lett.* **5** 1231–6
- [15] Huang J-S and Lin C-F 2008 Influences of ZnO sol-gel thin film characteristics on ZnO nanowire arrays prepared at low temperature using all solution-based processing *J. Appl. Phys.* **103** 014304
- [16] Neykova N, Hruska K, Holovsky J, Remes Z and Vanecek M 2013 Arrays of ZnO nanocolumns for 3-dimensional very thin amorphous and microcrystalline silicon solar cells *Thin Solid Films* **2–5**
- [17] Park H, Chang S, Jean J, Cheng J J, Araujo P T, Wang M, Basendi M G, Dresselhaus M S, Bulovic V, Kong J and Gradecak S 2012 Graphene cathode-based ZnO nanowire hybrid solar cells *Nano Lett.* **13** 233–9
- [18] Chen J, Lei W, Li C, Zhang Y and Cui Y 2011 Flexible quantum dot sensitized solar cell by electrophoretic deposition of CdSe quantum dots on ZnO nanorods *w* 13182–4
- [19] Johnston K W, Pattantyus-Abraham A G, Clifford J P, Myrskog S H, Hoogland S, Shukla H, Klem E J D, Levina L and Sargent E H 2008 Efficient Schottky-quantum-dot photovoltaics: The roles of depletion, drift, and diffusion *Appl. Phys. Lett.* **92** 122111
- [20] Kramer I J, Zhitomirsky D, Bass J D, Rice P M, Topuria T, Krupp L, Thon S M, Ip A H, Debnath R, Kim H and Sargent E H 2012 Ordered Nanopillar Structured Electrodes for Depleted Bulk Heterojunction Colloidal Quantum Dot Solar Cells *Adv. Mater.* **24** 2315–9
- [21] Richardson J J, Estrada D, DenBaars S P, Hawker C J and Campos L M 2011 A facile route to patterned epitaxial ZnO nanostructures by soft lithography *J. Mater. Chem.* **21** 14417
- [22] Xu S, Wei Y, Kirkham M, Liu J, Mai W, Davidovic D, Snyder R L and Wang Z L 2008 Patterned Growth of Vertically Aligned ZnO Nanowire Arrays on Inorganic Substrates at Low Temperature without Catalyst *J. Am. Chem. Soc.* **130** 14958–9
- [23] Lee W W, Yi J, Kim S B, Kim Y-H, Park H-G and Park W Il 2011 Morphology-controlled three-dimensional nanoarchitectures produced by exploiting vertical and in-plane crystallographic orientations in hydrothermal ZnO crystals *Cryst. Growth Des.* **11** 4927–32
- [24] Weintraub B, Deng Y and Wang Z L 2007 Position-Controlled Seedless Growth of ZnO Nanorod Arrays on a Polymer Substrate via Wet Chemical Synthesis *J. Phys. Chem. C* **111** 10162–5
- [25] Zhang D, Wang S, Cheng K, Dai S, Hu B, Han X, Shi Q and Du Z 2012 Controllable fabrication of patterned ZnO nanorod arrays: investigations into the impacts on their morphology *Appl. Mater. Interfaces* **4** 2969–77
- [26] Erdelyi R, Nagata T, Rogers D J, Teherani F H, Horvath Z E, Labadi Z, Baji Z, Wakayama Y and Volk J 2011 Investigations into the Impact of the Template Layer on ZnO Nanowire Arrays Made Using Low Temperature Wet Chemical Growth *Cryst. Growth Des.* **11** 2515–9
- [27] Song J and Lim S 2007 Effect of Seed Layer on the Growth of ZnO Nanorods *J. Phys. Chem. C* **111** 596–600

- [28] Cross R, De Souza M and Narayanan E 2005 A low temperature combination method for the production of ZnO nanowires *Nanotechnology* **16** 2188–92
- [29] Ma T, Guo M, Zhang M, Zhang Y and Wang X 2007 Density-controlled hydrothermal growth of well-aligned ZnO nanorod arrays *Nanotechnology* **18** 035605 – 035612
- [30] Tian Z R, Voigt J A, Liu J, Mckenzie B, McDermott M J, Rodriguez M A, Konishi H and Xu H 2003 Complex and oriented ZnO nanostructures *Nat. Mater.* **2** 821–6
- [31] Fan H J, Lee W, Hauschild R, Alexe M, Rhun L, Scholz R, Dadgar A, Nielsch K, Kalt H, Krost A, Zacharias M and Gçsele U 2006 Template-Assisted Large-Scale Ordered Arrays of ZnO Pillars for Optical and Piezoelectric Applications 561–8
- [32] Joo J, Chow B Y, Prakash M, Boyden E S and Jacobson J M 2011 Face-selective electrostatic control of hydrothermal zinc oxide nanowire synthesis. *Nat. Mater.* **10** 596–601
- [33] Lin M, Wang Y, Chen H, Alejandro J M, Su C and Jeng U 2011 Critical analysis of the crystal orientation behavior in polyethylene-based crystalline-amorphous diblock copolymer *J. Phys. Chem. B* **115** 2494–502
- [34] Wu H, Wang W, Huang Y and Su Z 2009 Orientation of syndiotactic polystyrene crystallized in cylindrical nanopores. *Macromol. Rapid Commun.* **30** 194–8
- [35] Wei Y, Wu W, Guo R, Yuan D, Das S and Wang Z L 2010 Wafer-scale high-throughput ordered growth of vertically aligned ZnO nanowire arrays. *Nano Lett.* **10** 3414–9
- [36] Zhang S, Shen Y, Fang H, Xu S and Lin Z 2010 Growth and replication of ordered ZnO nanowire arrays on general flexible substrates *J. Mater. Chem.* **20** 10606–10
- [37] Nagata T, Rogers D J, Teherani F H, Horv Z E and Wakayama Y 2011 Investigations into the Impact of the Template Layer on ZnO Nanowire Arrays Made Using Low Temperature Wet Chemical Growth 2515–9
- [38] Li C, Hong G, Wang P, Yu D and Qi L 2009 Wet chemical approaches to patterned arrays of well-aligned ZnO nanopillars assisted by monolayer colloidal crystals *Chem. Mater.* **21** 891–7
- [39] Kim T, Kim J, Pawar S M, Moon J and Kim J H 2010 Creation of Nanoscale Two-Dimensional Patterns of ZnO Nanorods using Laser Interference Lithography Followed by Hydrothermal Synthesis at 90 ° C *Cryst. Growth Des.* **10** 4256–61
- [40] Chao C, Huang J and Lin C 2009 Low-Temperature Growth of Surface-Architecture-Controlled ZnO Nanorods on Si *J. Phys. Chem. C* **113** 512–7
- [41] Tao Y, Fu M, Zhao A, He D and Wang Y 2010 The effect of seed layer on morphology of ZnO nanorod arrays grown by hydrothermal method *J. Alloys Compd.* **489** 99–102
- [42] Richardson J J, Estrada D and DenBaars 2011 A facile route to patterned epitaxial ZnO nanostructures by soft lithography *J. Mater. Chem.* **21** 14417–9

- [43] Li H, Low J, Brown K S and Wu N 2008 Large-Area Well-Ordered Nanodot Array Pattern Fabricated With Self-Assembled Nanosphere Template *IEEE Sens. J.* **8** 880–4
- [44] Korre H, Fucetola C P, Johnson J a. and Berggren K K 2010 Development of a simple, compact, low-cost interference lithography system *J. Vac. Sci. Technol. B Microelectron. Nanom. Struct.* **28** C6Q20
- [45] Qin Y, Wang X and Wang Z L 2008 Microfibre-nanowire hybrid structure for energy scavenging. *Nature* **451** 809–13
- [46] Li S, Hu J, Li J, Tian J, Han Z, Zhou X and Chen Y 2011 Anisotropic Wet Etched Silicon Substrates for Reoriented and Selective Growth of ZnO Nanowires and Enhanced Hydrophobicity *Langmuir* **27** 6549–53
- [47] Goldberger J, Sirbuly D J, Law M and Yang P 2005 ZnO Nanowire Transistors *J. Phys. Chem. B* **109** 9–14
- [48] Chen A, Chua S J, Chen P, Chen X Y and Jian L K 2006 Fabrication of sub-100 nm patterns in SiO<sub>2</sub> templates by electron-beam lithography for the growth of periodic III–V semiconductor nanostructures *Nanotechnology* **17** 3903–8